We are IntechOpen, the world's leading publisher of Open Access books
Built by scientists, for scientists

4,800
Open access books available

122,000
International authors and editors

135M
Downloads

Our authors are among the

154
Countries delivered to

TOP 1%
most cited scientists

12.2%
Contributors from top 500 universities

CLARIVATE ANALYTICS
BOOK CITATION INDEX
INDEXED

WEB OF SCIENCE™

Selection of our books indexed in the Book Citation Index in Web of Science™ Core Collection (BKCI)

Interested in publishing with us?
Contact book.department@intechopen.com

Numbers displayed above are based on latest data collected.
For more information visit www.intechopen.com

Proton Exchange Membrane Water Electrolysis as a Promising Technology for Hydrogen Production and Energy Storage

Radenka Maric and Haoran Yu

Additional information is available at the end of the chapter

http://dx.doi.org/10.5772/intechopen.78339

Abstract

Proton exchange membrane (PEM) electrolysis is industrially important as a green source of high-purity hydrogen, for chemical applications as well as energy storage. Energy capture as hydrogen via water electrolysis has been gaining tremendous interest in Europe and other parts of the world because of the higher renewable penetration on their energy grid. Hydrogen is an appealing storage medium for excess renewable energy because once stored, it can be used in a variety of applications including power generation in periods of increased demand, supplementation of the natural gas grid for increased efficiency, vehicle fueling, or use as a high-value chemical feedstock for green generation of fertilizer and other chemicals. Today, most of the cost and energy use in PEM electrolyzer manufacturing is contributed by the cell stack manufacturing processes. Current state-of-the-art electrolysis technology involves two options: liquid electrolyte and ion exchange membranes. Membrane-based systems overcome many of the disadvantages of alkaline liquid systems, because the carrier fluid is deionized water, and the membrane-based cell design enables differential pressure operation.

Keywords: hydrogen, renewable energy, proton exchange membrane (PEM) water electrolysis, nanostructure, oxygen evolution reaction (OER)

1. Hydrogen as a future energy carrier

Eighty-five percent of the energy consumed globally is provided by fossil fuels, namely coal, oil, and natural gas [1]. Fossil fuels come from finite resources which will eventually become scarce and difficult to explore. Thus, fossil fuels are considered nonrenewable energy sources [2]. Furthermore, consuming fossil fuels produces greenhouse gases and other byproducts, causing

climate change and air pollution. The growing demand for energy requires a rapid shift from fossil fuels to renewable energy sources, such as wind, solar, biomass, hydropower, and geothermal energy [3]. In this context, hydrogen was proposed as a promising candidate for a secondary source of energy as early as 1973 [4]. Being a potential energy carrier in the future, hydrogen plays an important role in the path toward a low-carbon energy structure that is environmentally friendly [5–10].

## 1.1. Hydrogen production from renewable energy sources

Currently, the steam reforming process is the most economical way of producing hydrogen. In fact, as much as 96% of hydrogen is made from hydrocarbon fuels [5], which neither address the dependence on finite resources nor reduce the amount of carbon from the energy structure. An alternative way of producing hydrogen is the power-to-gas strategy where intermittent energy resources are transferred and stored as hydrogen (**Figure 1**). Here, hydrogen is mainly produced from water electrolysis where water is split into hydrogen and oxygen by supplying electrical energy:

$$H_2O \xrightarrow{electricity} H_2 + \frac{1}{2}O_2 \tag{1}$$

In an electrolyzer, the above reaction is separated by an electrolyte (either in liquid or solid form) into two half reactions. The hydrogen evolution reaction (HER) occurs at the cathode:

$$2H^+ + 2e^- \rightarrow H_2\uparrow, E^0 = 0.0\ V \tag{2}$$

While the oxygen evolution reaction (OER) occurs at the anode:

$$H_2O \rightarrow 2H^+ + 2e^- + \frac{1}{2}O_2\uparrow, E^0 = 1.23\ V \tag{3}$$
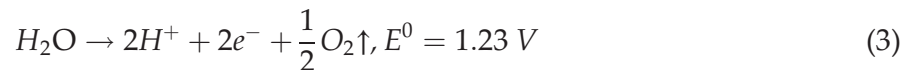
Water electrolysis technologies are classified into three categories based on the applied electrolyte: alkaline water electrolysis, proton exchange membrane (PEM) water electrolysis, and solid oxide water electrolysis [11]. PEM water electrolysis systems provide several advantages over the other two electrolysis technologies, such as higher rate of hydrogen production, more compact design, and greater energy efficiency [12–15]. Compared to alkaline electrolysis, the solid electrolyte membrane in PEM electrolysis reduces the hydrogen crossover significantly and thus allows for high-pressure operation. In addition, as required by the role of electrolytic hydrogen production in renewable energy storage, dynamic response of PEM water electrolysis is superior to alkaline electrolysis or solid oxide electrolysis. The large quantity of liquid electrolyte in alkaline electrolysis requires the proper temperature to be maintained and could raise issues for a cold start. On the other hand, solid oxide electrolysis operated in a temperature range of 500–700°C is more suitable for constant operation than a dynamic response where the heat-up step could be slow.

The produced hydrogen can have several pathways to different applications (**Figure 1**). It can be utilized for hydrogen fueling stations to power fuel cell vehicles or feed the combined heat and power (CHP) units for household uses. Moreover, the electrolytic hydrogen can be used as
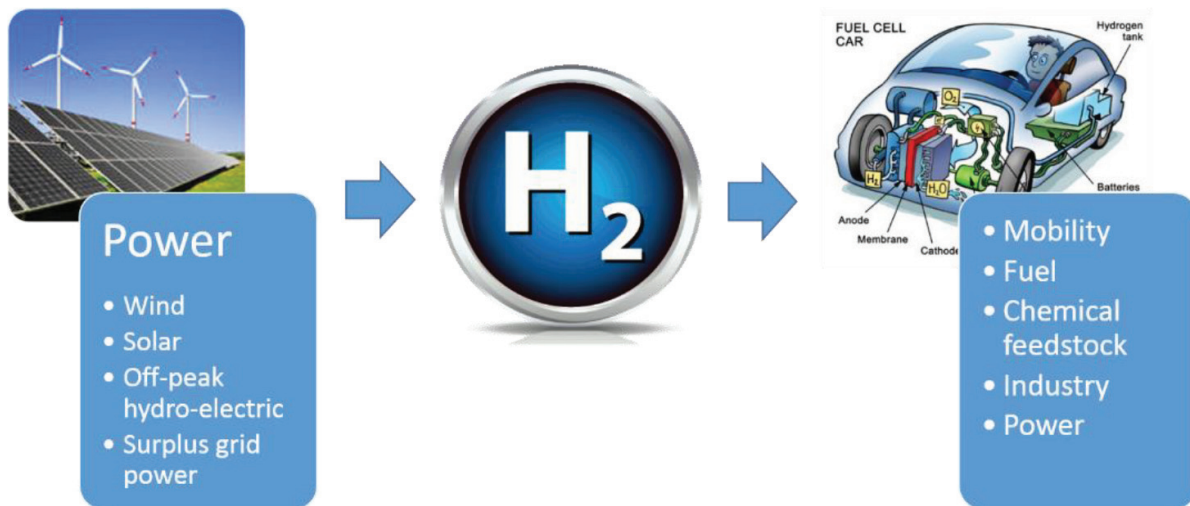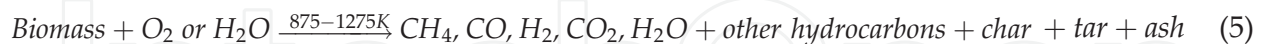
Figure 1. Schematic diagram of power-to-gas strategy.

chemical feedstock in methanation after combining with CO_2 stream from biogas or flue gas to produce renewable natural gas. Further, the generated hydrogen can also be consumed as a raw material by hydrogen users such as oil refining and semiconductor industry. Finally, the hydrogen can be transferred to electricity when the grid demand is high.

Hydrogen can also be produced from biomass via pyrolysis or gasification. Wood, agricultural crops and its byproducts, organic waste, animal waste, waste from food processing, and so on are all sources of biomass. Biomass pyrolysis is basically [9]:

$$Biomass + Heat \xrightarrow{625-775K,\, 1-5\ bar} CH_4 + CO + H_2 + other\ products \tag{4}$$

Employing catalysts, such as Ni-based catalysts, can enhance the yield of hydrogen from biomass pyrolysis. Moreover, hydrogen production can be improved by introducing steam reforming and water-gas shift reaction to the pyrolysis [9]. For the gasification process, biomass is pyrolyzed at higher temperatures producing mostly gaseous products [9]:

$$Biomass + O_2\ or\ H_2O \xrightarrow{875-1275K} CH_4, CO, H_2, CO_2, H_2O + other\ hydrocarbons + char\ + tar + ash \tag{5}$$

It is beneficial that biomass pyrolysis and gasification can be operated in small scale and at remote locations, which reduces the cost of hydrogen transportation and storage and improves the availability of hydrogen to end consumers [16]. In addition, pyrolysis and gasification can consume a wide range of biomass feedstocks [16]. Therefore, biomass is recognized as a major renewable and sustainable energy source to replace fossil fuel.

1.2. Hydrogen storage

Currently, hydrogen storage in high-pressure vessel is the most widely used method [7]. However, hydrogen is pressurized up to 700 bar for practical purposes such as the refueling time at a hydrogen station or the driving range for a fuel cell vehicle [17]. Hydrogen compression to 700 bar consumes a lot of energy that makes the volumetric energy density decrease

from 10 to 5.6 MJ/L, much lower than gasoline (34 MJ/L) [6, 17]. Therefore, solid-state storage is usually coupled with high-pressure hydrogen vessels. For example, hydrogen can be stored in the interstitial sites of metal hydride crystals [17]. This method achieves higher volumetric energy density at room temperature than liquid hydrogen and consumes less operating energy for storage. Thus, metal hydride cartridge is suitable for portable application due to the convenience of refill/replace [7, 18]. In addition, with appropriate hydrogen refill and release properties at room temperature, metallic hydrides are good for stationary energy storage [17]. One drawback of solid-state storage is that metallic hydrides contain heavy transition metals, which reduce the gravimetric energy density of the device [19].

In summary, hydrogen offers several advantages as an energy carrier: its combustion produces energy and only water that is carbon-free as a byproduct; it can be produced from renewable and sustainable sources; its energy can be distributed quite easily, in accordance with the end user's requests and with the development of new technologies for transportation and storage; it may be used in both centralized or distributed energy production [7]. In spite of these advantages, hydrogen has failed to be widely used in energy systems due to numerous barriers, including costs of production and storage and the availability of infrastructure [10]. This chapter focuses on the technological challenges of PEM water electrolyzers for hydrogen production.

2. Introduction of PEM water electrolysis

2.1. Fundamentals of PEM water electrolysis

Figure 2 shows the schematic diagram of PEM water electrolysis. The electrolysis process is an endothermic process and electricity is applied as the energy source. The water electrolysis reaction is thermodynamically possible at potentials higher than 1.23 V vs. RHE (reversible hydrogen electrode). The thermoneutral potential at which the cell can operate adiabatically is 1.48 V vs. RHE. Typical PEM water electrolysis devices operate at potential well over 1.48 V vs. RHE and heat is generated by the reaction [15]. The PEM water electrolysis system, similar to proton exchange membrane fuel cell (PEMFC), anode and cathode is separated by a solid polymer electrolyte (Nafion) of thickness below 0.2 mm. At the anode, water is oxidized to produce oxygen, electrons, and protons. The protons are transported across the electrolyte membrane to be reduced to hydrogen. The catalyst for water oxidation or oxygen evolution is typically iridium, which can withstand the corrosive environment due to high overpotential on the anode. Water is channeled to the anode by a titanium flow field, and a piece of porous titanium mesh is placed between the anode catalyst layer and the water channel serving as the diffusion layer. The cathode configuration is similar to the PEMFC with Pt-based catalyst and a graphite flow field to transport hydrogen. A piece of carbon paper is used as the gas diffusion layer (GDL) placed between the cathode catalyst and the flow field.

The hydrogen production rate of ideal electrolysis is proportional to the charge transferred, according to Faraday's law. It can be expressed as [20]:
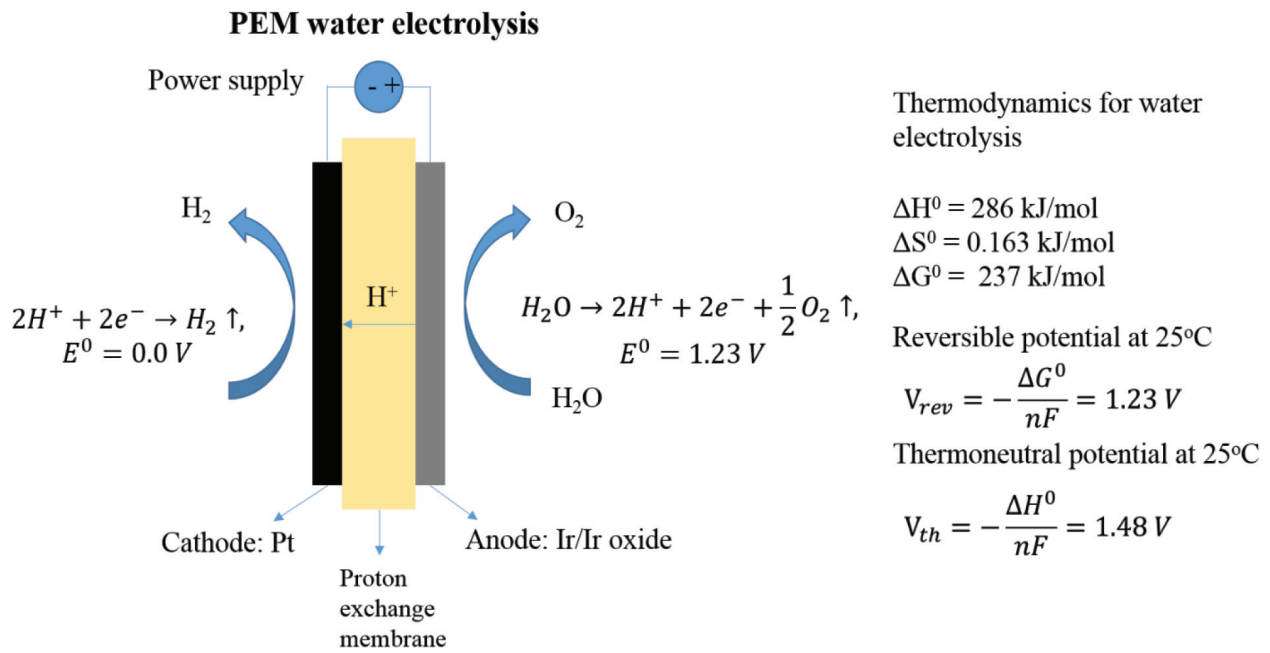
PEM water electrolysis

Figure 2. Schematic diagram of PEM water electrolysis and the fundamental thermodynamic properties.

$$f_{H_2} = \eta_F \frac{N_{Cell} I_{Cell}}{zF} \frac{22.41}{1000} 3600 \tag{6}$$

where N_{cell} is the total number of cells in the system and I_{cell} is the electric current. η_F is the Faraday efficiency, or current efficiency, and is defined as the ratio of ideal electric charge and the practical charge consumed by the device when a certain amount of hydrogen is generated. η_F is usually about 0.95 [20]. The specific energy consumption E (kWh/Nm³) for a given time interval Δt is:

$$E = \frac{\int_0^{\Delta t} N_{cell} I_{cell} V_{cell} dt}{\int_0^{\Delta t} f_{H2} dt} \tag{7}$$

Another important parameter for PEM water electrolysis is the efficiency:

$$\eta = \frac{HHV}{E} \tag{8}$$

where HHV is the higher heating value of hydrogen (39.4 kWh/kg at STP). Since PEM water electrolysis is usually supplied by liquid water, the HHV assumes that all the heat from the water is recovered by restoring the water temperature to the initial ambient state [20].

2.2. Challenges for PEM water electrolysis: the OER catalyst

Significant advances are needed in catalyst and membrane materials as well as the labor-intensive manufacturing process for PEM water electrolysis to be cost-effective for widespread application in renewable energy systems [21]. The state-of-the-art anode catalyst in

References	Anode catalyst	Ir loading, mg cm^{-2}	Cathode catalyst	Pt loading, mg cm^{-2}	Electrode fabrication process	Active area	Test period, hours	Operating temperature, °C	Operating current, A cm^{-2}	Test period, hours	Degradation rate, μV h^{-1}
Grigoriev et al. [40]	Ir black	1.5	Pt/Vulcan XC-72	1.0	Spraying	25	4000	60	0.5	4000	35.5
Rozain et al. [41]	IrO$_2$/Ti	0.12	Pt/C, TKK	0.25	Spraying	25	1000	80	1	1000	27
Rozain et al. [41]	IrO$_2$	0.32/0.1	Pt/C, TKK	0.25	Spraying	25	1000	80	1	1000	110/180[*]
Siracusano et al. [42]	IrO$_2$	0.4	Pt/Vulcan XC-72	0.1	Spray-coating	5	1000	80	1.0	1000	12
Rakousky et al. [43]	IrO$_2$ and TiO$_2$	2.25	Pt/C	0.8	Commercial	17.64	1150	80	2.0	1150	194
Lettenmeier et al. [44]	Ir black	1	Pt black	0.9	Commercial	120	400	55–60	2.0	400	Not significant
Lewinski et al. [45]	Ir-NSTF	0.25	Pt-NSTF	0.25	3 M	50	5000	80	2	5000	Average 6.8
RSDT Cell-4	IrOx and Nafion	0.08	Pt/Vulcan XC-72R	0.3	RSDT	86	4543	80	1.8	4543	36.5–48.7, 11.5
Wang et al. [46]	Ir$_{0.7}$Ru$_{0.3}$Ox	1[**]	Pt/C	0.4	Air-brush spraying	25	400	80	1	400	Not significant
Siracusano et al. [47]	Ir$_{0.7}$Ru$_{0.3}$Ox	0.34[**]	Pt/Vulcan XC-72	0.1	Electrode fabrication process	Active area	1.0/3.0	80	1.0/ 3.0	1000	15/23[***]

[*]Degradation rate at 0.32 and 0.1 mg cm^{-2} Ir loading, respectively.

[**]Loading of Ir and Ru combined.

[***]Degradation rate at 1.0 and 3.0 A cm^{-2}, respectively.

Table 1. Reported degradation rates for iridium-based catalysts in long-term electrolyzer tests.

conventional PEMWEs is iridium oxide (IrOx) or mixed oxide with ruthenium [22, 23]. Typical catalysts for commercial electrodes have IrOx loading from 1 to 3 mg cm^{-2} [24]. This level of catalyst loading is too high to meet the long-term cost targets for energy markets [23, 25, 26]. Furthermore, while using current electrolysis technology, the translation of catalyst development from lab scale to the megawatt scale remains challenging in terms of catalyst cost and stability [25].
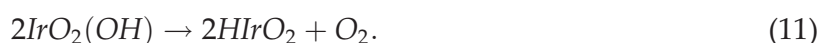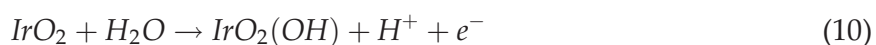
For Ir- and Ru-based OER catalyst, a balance between activity and stability has been reported [27, 28], which strongly depends on the chemical structure and surface properties of the oxide [23]. The oxide properties, however, are highly sensitive to synthesis conditions. For Ir-based OER catalyst, most synthesis methods involve a calcination step to improve the catalyst stability [29–35]; however, for this approach, a sacrifice of the OER activity is usually inevitable. Indeed, thermally prepared IrOx shows higher stability but lower activity compared to electrochemically prepared oxide, or hydrous IrOx [30, 31, 35]. The latter is also frequently referred to as amorphous IrOx due to the presence of lower valence Ir (III) oxide [36–38]. According to reference [39], Ir (III) is the major intermediate species for iridium dissolution. Combining both activity and stability remains a challenge for Ir-based catalysts, and it is the major hurdle that limits the reduction of the anode iridium loading in PEM water electrolysis.

The enhancement of catalyst stability is of equal importance as the reduction of catalyst loading. Long-term operation at high current density up to thousands of hours is particularly challenging with an Ir loading less than 1 mg cm^{-2}. Recent literature has seen a growing number of studies on longer-term electrolysis operation ranging from hundreds to several thousand hours [40–47] (**Table 1**). In particular, the best reported stability was on a nanostructured thin film (NSTF) cell, which achieved 5000 hours with a constant current load of 2 A cm^{-2} and 0.25 mg cm^{-2} Ir loading [45]. IrOx supported on Ti catalyst with 50 wt% Ir and a low catalyst loading of 0.12 mg cm^{-2} achieved more than 1000 hours operation at a lower current load of 1 A cm^{-2} [41]. No supported catalyst, other than titanium supported catalyst has been able to achieve such high catalyst stability. [48]

3. The role of nanostructures in PEM electrolyzer performance

3.1. The structure of iridium oxide (IrOx)

The OER performance of IrOx strongly depends on the chemical structure and surface properties of the oxide [23]. Before discussing the influence of oxide structure on the electrolyzer performance, a thorough understanding of the OER mechanism is needed. The OER on IrOx consists of three steps forming a closed circle (**Figure 3**) [39, 49, 50]:

$$HIrO_2 \rightarrow IrO_2 + H^+ + e^- \tag{9}$$

$$IrO_2 + H_2O \rightarrow IrO_2(OH) + H^+ + e^- \tag{10}$$

$$2IrO_2(OH) \rightarrow 2HIrO_2 + O_2. \tag{11}$$

Reaction (9) is fast and in pre-equilibrium. Reaction (10) is the rate-determining step (RDS), and the theoretical Tafel slope of this mechanism is 2RT/3F = 40 mV/dec. Since it is noted that Eq. (11) involves two iridium sites, a binuclear mechanism of OER on IrOx is proposed for Eq. (11) [51]. With the aid of density functional theory (DFT) calculations, Steesgra et al. [52] show that the first step of the binuclear mechanism is the oxidation of Ir (IV) – Ir (IV) to Ir (IV) – Ir (V), which is Eq. (10). Therefore, $IrO_2 \cdot H_2O$ is considered to be the precursor for the binuclear mechanism. The coverage of Ir (V) increases with the anodic potential until the conditions for the binuclear mechanism are satisfied [39] at the onset of OER.

In a series of studies of iridium dissolution [31, 32, 39, 53], it is proposed that the precursor for dissolution are the oxygenated Ir (III) species (**Figure 3**). The formation and reduction of higher valence Ir (IV) species pass through an Ir (III) intermediate, which is shared in both OER and iridium dissolution. It is concluded in [39] that iridium dissolution has no direct link with OER activity and that they are two pathways sharing an intermediate species, Ir (III). Thus, it is possible to suppress one without alternating the other [39]. Therefore, the ratio of Ir (IV) to Ir (III) on the IrOx surface is a crucial parameter that controls the iridium dissolution and the OER.

Amorphous and nano-sized IrOxs have received much attention as promising OER catalysts due to the co-existence of Ir (III) and Ir (IV) oxidation state [35–38, 54–56], forming an oxide termed "iridium oxohydroxide." For example, using X-ray absorption spectroscopy (XAS) and X-ray absorption near edge spectroscopy (XANES), Minguzzi et al. [37, 38] confirms the co-existence of Ir (III) and Ir (IV) at anodic potentials where OER occurs. However, this does not imply that a mixed IrOx state fundamentally leads to high OER activity. In fact, the OER mechanism (Eqs. (9)–(11)) predicts that Ir (III) and Ir (IV) would certainly co-exist as Eqs. (9)–(11) form a loop. The higher OER activity of mixed Ir (III) and Ir (IV) oxides have been attributed to the presence of electrophilic O^{I-} species [57–61]. Electrophilic O^{I-} is the precursor for the O-O bond formation according to the binuclear mechanism [52]. The oxygen 2p state probed with near-edge X-ray absorption fine structure (NEXAFS) suggests that electrophilic O^{I-} has a lower energy state compared to the O^{II-} species [61]. The weakly bonded O^{I-} is susceptible to nucleophilic attack from the pre-adsorbed water or hydroxyl groups, promoting the formation of O-O
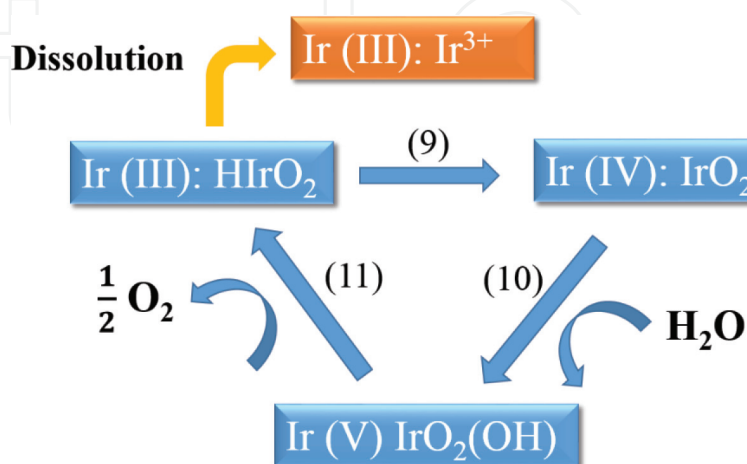

Figure 3. Circle of oxygen evolution: Eqs. (9)–(11).

bond [58, 59]. Calcination at a high temperature of "dry" IrOx (O^{II-} species) where electrophilic O^{I-} becomes strongly bonded O^{II-} species and thus the OER activity is reduced [36], in agreement with other studies [30, 31, 35, 62]. However, the "dry" IrOx is more stable against dissolution as the Ir (III) species on the surface is reduced [32, 60].

In addition, the IrOx structure can be modified when a metal oxide support is incorporated with IrOx nanoparticles via the metal/metal oxide support interaction. For example [63], when IrO_2 nanoparticles are supported on antimony-doped tin oxide (ATO), the d band vacancy and iridium oxidation decreased due to the interfacial electron charge donation from ATO to iridium, evidenced by the shift of X-ray absorption white line toward lower energy. This is corroborated with the increased Ir-O bonding distances for ATO-supported IrOx from extended X-ray fine structure (EXAFS) analysis, which is consistent with a lower average iridium oxidation state. Such interaction between IrOx and ATO suppressed the growth of higher valent IrOx layer that leads to iridium dissolution, thereby improved catalyst stability [63]. Similar interaction between metal/metal oxide supports was also found for IrO_2 supported on TiO_2 catalyst where the catalyst stability was enhanced as well [64].

3.2. Mixed bimetallic oxide

Mixed bimetallic oxides of iridium and a non-noble metal have been used to optimize the anode catalyst for PEM electrolyzer application [65–73]. The most apparent benefit of bimetallic oxide is to reduce the iridium loading in the catalyst if the catalyst activity remains comparable or higher compared to pure IrOx. For example, at >10 mol% iridium content in $IrO_2 + SnO_2$ mixed oxide the Tafel slope for OER is identical with pure IrO_2, suggesting that the surface properties of $IrO_2 + SnO_2$ mixed oxide is dominated by IrO_2 and behave as pure IrO_2 [65]. In particular, iridium content in the 30–90 mol% range shows higher OER performance than pure IrO_2 [65].

More importantly, mixed bimetallic oxides modify the electronic or crystal structures of IrOx, which can significantly enhance the OER activity. The bond forming or breaking during OER is governed by the interaction between the O-2p orbital of intermediates with the d orbitals of surface sites of the transition metals [66–68, 70–73]. Thus, the OER activity depends on the d-orbital electronic structure of the transitional metals. For example, Sun et al. [73] doped IrOx with copper and obtained enhanced OER activity in acid media at 30–50 mol% concentration. The Cu doping led to an IrO_2 lattice distortion due to the CuO_6 octahedron's Jahn-Teller effect and also generated oxygen defects (**Figure 4a**), which significantly affected the energy distribution of the d-orbitals of Ir sites. The induced partial oxygen defects and the lifted degeneracy of t_{2g} and e_g orbitals reduced the energy required for the O-O bond formation, thereby enhanced the OER activity. In another case, Reier et al. [69] prepared Ir-Ni mixed oxide thin film and found a 20-fold enhancement of OER activity compared to pure IrOx thin film. As shown in **Figure 4b**, the surface Ni elements are leached out during OER and weakened the binding energy of the Ni-depleted oxygen with the lattice, forming oxygen with lower binding energy, and similar to the electrophilic oxygen. This promotes the formation of weakly bonded surface hydroxyls, which govern the overall OER reaction rate and suppress the formation of unreactive divalent = O species on the surface. Furthermore, Tae et al. [70] reported Ir-Co mixed oxide with 5% iridium
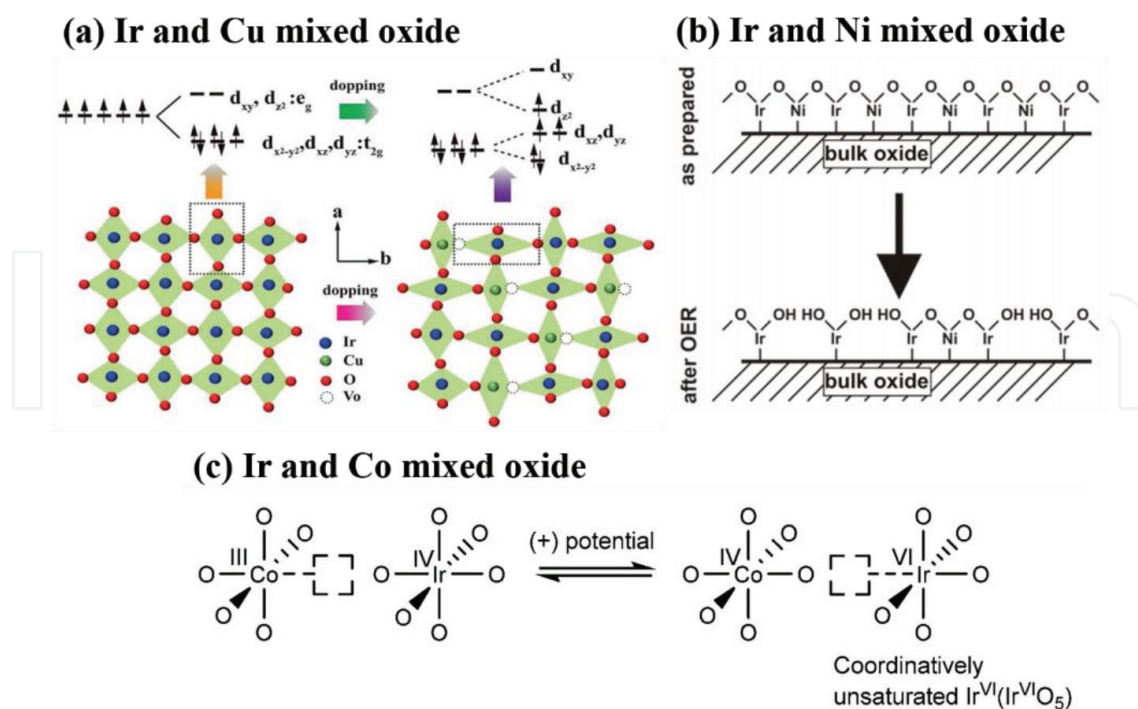
Figure 4. (a) Schematic lattice diagram in the ab plane of IrO$_2$ (left) and substituted by Cu (right). The top row shows Ir-5d orbitals degeneracy of IrO$_2$ (left) and the lift degeneracy and electron redistribution by doping with Cu [73]—Published by The Royal Society of Chemistry. (b) Model of Ni-leaching during OER for Ir-Ni mixed oxide surface, reproduced with permission [69]. Copyright (2015) American Chemical Society. (c) Transfer of oxygen vacancy from Co (III) to Ir (VI), reproduced with permission [70]. Copyright (2015) American Chemical Society.

loading that exhibits excellent OER activity and stability. At anodic potentials, the oxygen vacancy in Co (III) is transferred to Ir (IV) O$_6$ center, leading to the formation of coordinatively unsaturated Ir (VI) O$_5$ structure (**Figure 4c**), which is highly active for OER.

3.3. Effect of particle size

Small particles are usually favorable for higher mass activity due to the high surface area to bulk ratio, which facilitates the reduction of catalyst loading. More importantly, the change of electronic structure is unavoidably accompanied with the change of particle size, as evidenced in the early work on X-ray photoelectron spectroscopy (XPS) [74–76]. As particle size decreases, the binding energy is shifted to higher levels due to the increase of lattice strain and the coordination reduction [77, 78]. Richter et al. [78] shows that two mechanisms contribute to such an energy shift. The first is the initial state effect caused by the increase of lattice strain as particle size decreases, a result of d-hybridization; the second is the final state relaxation that increases with the decrease of particle size, which results in the stronger screening of the core hole leading to higher binding energy. Small particles show enhanced d-hybridization, which shift the d-band center to lower levels, decreasing the bond strength of the adsorbates during an electrochemical reaction [79].

Abbot et al. [34] systematically studied the particle size effect for IrOx in the range of 2 –30 nm. EXAFS analysis reveals that, as the IrOx particle size decreases, the coordination number

decreases and the Ir-O bond length increases. The core-level binding energy was thus shifted to higher levels as the particle size decreases, which is in agreement with previous literature [74–76]. As a result, the iridium-oxygen bonding is weakened as the particle size decreases, leading to higher content of hydroxide, and lower average oxidation state of iridium from Ir (IV) to a combination of Ir (IV) and Ir (III). Based on previous discussions in Section 3.1, surface hydroxide and mixed Ir (IV) and Ir (III) state are favorable for OER. Indeed, Abbot et al. [34] show that the IrOx particles of 2 nm have 10 fold higher OER mass activity and three fold higher turnover frequency compared to the IrOx particles of 30 nm.

3.4. Effect of ionomer content

Perfluorosulfonic acid ionomer provides proton conductivity in the catalyst layer, extends the reaction zone, and improves the catalyst utilization [80, 81]. Ma et al. [82] focused on the effect of ionomer content on the ohmic resistance of PEM electrolyzers with iridium supported on titanium carbide (TiC) as an anode catalyst. Ma et al. [82] showed that increasing the ionomer content from 10 to 40 wt% causes a decrease in PEMWE performance. Using a simple non-linear fit:

$$E_{corrected} = E_{applied} - IR = a + b\ logI \qquad (12)$$

The authors derived the ohmic loss contribution in the performance and concluded that higher ohmic resistance is associated with high ionomer content. It is noted that with this non-linear fit method, the obtained ohmic resistance includes contributions from all sources of the membrane electrode assembly (MEA) components, including the ionic resistance. Xu et al. [83] investigated the effect of ionomer content from the voltammetric charge and interfacial resistance perspective. The amount of voltammetric charges in cyclic voltammetry is proportional to the surface active sites [84]. A wider range of ionomer contents, from 5 to 40 wt%, were studied. The highest total charge was achieved at 25 wt% ionomer content, which is in agreement with the optimum PEMWE performance. Based on Butler-Volmer equation, the authors constructed a model to describe the I-V curves and concluded that the optimum ionomer content minimizes the interfacial resistance between the membrane and the electrode.

In a recent study, Bernt and Gasteiger [85] investigated the effect of anode ionomer content by analyzing the voltage loss contribution to the PEMWE performance. The ohmic resistance was found to increase abruptly when the ionomer content is above 20 wt%. This suggests that an electronically insulating film of residual ionomer forms at the electrode/GDL interface when the ionomer volume exceeds the void volume of the catalyst layer, which results in higher contact resistances. Further, such electronic insulation caused higher OER overpotential with >20 wt% ionomer content and thereby decreased the catalyst utilization. After subtracting the voltage losses due to ohmic and kinetic losses, Bernt and Gasteiger [85] attributed to the remaining losses (red diamond) to mass transport (**Figure 5**). The main path for oxygen removal from the electrode is not permeation but convective transport through the void volume of the anode. Thus, higher ionomer content imposes higher transport resistance for oxygen removal.

In sum, similar to PEM fuel cell electrodes, the ionomer content is an important parameter for the optimization of PEM electrolyzers. While low ionomer content provides insufficient proton
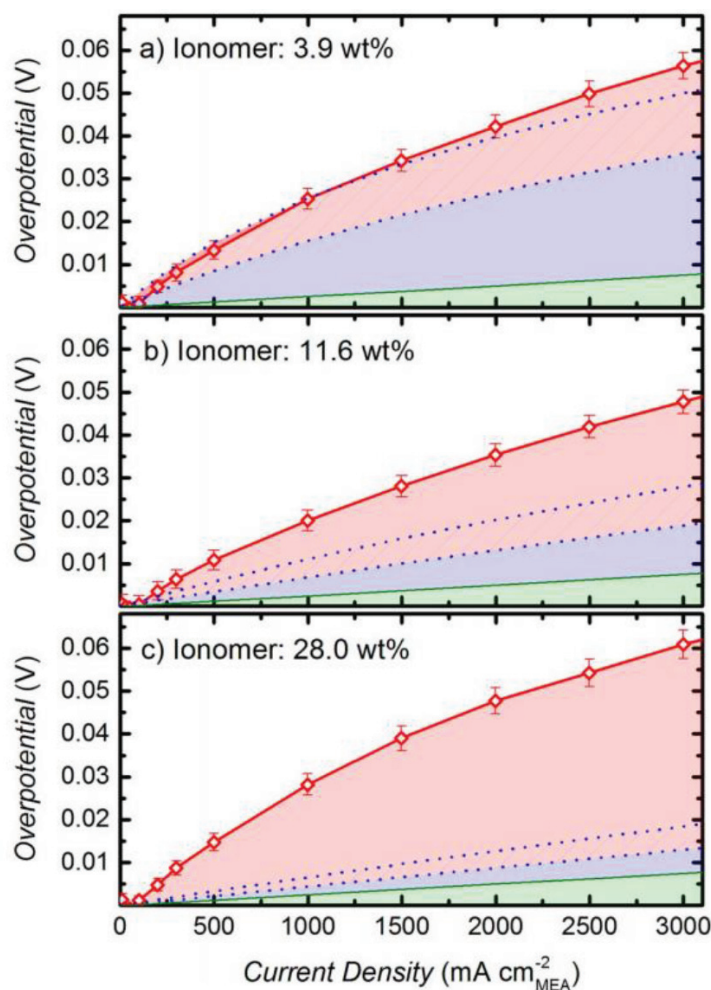
Figure 5. Overpotentials of PEM electrolyzer MEAs with different anode ionomer content after subtraction of ohmic and kinetics losses. Overpotentials from different sources are represented as different colors. Blue: anode proton conduction resistance; Green: cathode proton conduction resistance; Red: remaining overpotentials due to mass transport loss. Reproduced with permission [85]. Copyright (2016) The Electrochemical Society.

conduction and less accessible surface active sites, high ionomer content induces high interfacial resistance and mass transport loss due to insufficient void volume for oxygen diffusion. PEM electrolyzers are economically beneficial for a large-scale application operating at high current densities (>2 A cm^{-2}) and high pressures (30–45 bar). Thus, optimization of the ionomer content becomes crucial to minimize the cell potential loss at high current and pressure and improve cell efficiency.

4. PEM water electrolysis for energy storage

4.1. Integration with renewable energy technologies

Power generated from renewable energy sources, such as solar and wind, requires energy storage devices to balance its fluctuation and intermittence because of variable weather

conditions [86]. Hydrogen production by water electrolysis has been developed as an alternative technology for energy conversion and storage that can be fitted to renewable energy systems [87, 88]. This section will briefly introduce the role of PEM electrolyzers in power-to-gas, solar, and wind energy systems.

Power-to-gas is emerging as a novel energy storage method that uses the surplus electricity from the grid during off-peak periods and converts it to hydrogen through a water electrolysis process [89]. The key technology for this strategy is the electrolyzer, which bridges the power to utilization by producing hydrogen. Electrolyzers must meet the following requirements in order for power-to-gas to become efficient and economically viable [90]: (1) high efficiency of hydrogen production; (2) fast response to power fluctuation; (3) very low minimal load for stand-by; (4) high-pressure operation to reduce the cost of hydrogen compression; and (5) long durability and lifetime. The major drawback of power-to-gas is the low efficiency and high cost of electrolyzers. While PEM electrolyzers offer fast response, high pressure, and the production of pure hydrogen, scaling up to MW scale has been the major technical challenge. As mentioned previously, the major hurdle of this challenge is the cost of catalysts and other MEA components (e.g., the Ti-based bipolar plates).

Solar energy conversion into hydrogen by water splitting has been long studied by various research groups due to its easy scale-up nature. The state-of-the-art photocatalytic and photoelectrochemical system has an efficiency of 10 and 5%, respectively, in the direct conversion of solar to hydrogen (STH) [91]. To reduce the price of hydrogen and boost up the efficiency of STH, an electrolyzer cell (EC) can be coupled with a photovoltaic cell (PV), called photovoltaic–water electrolysis system (PV-EC) [92]. The STH efficiency can be increased up to 30%. Further, a direct current to direct current (DC-DC) converter can be implemented between PV and EC (**Figure 6**). The main role of the converter is maximum power point tracking of the sun light to the EC system. Thus, coupling electrolyzers with highly efficient PVs and with
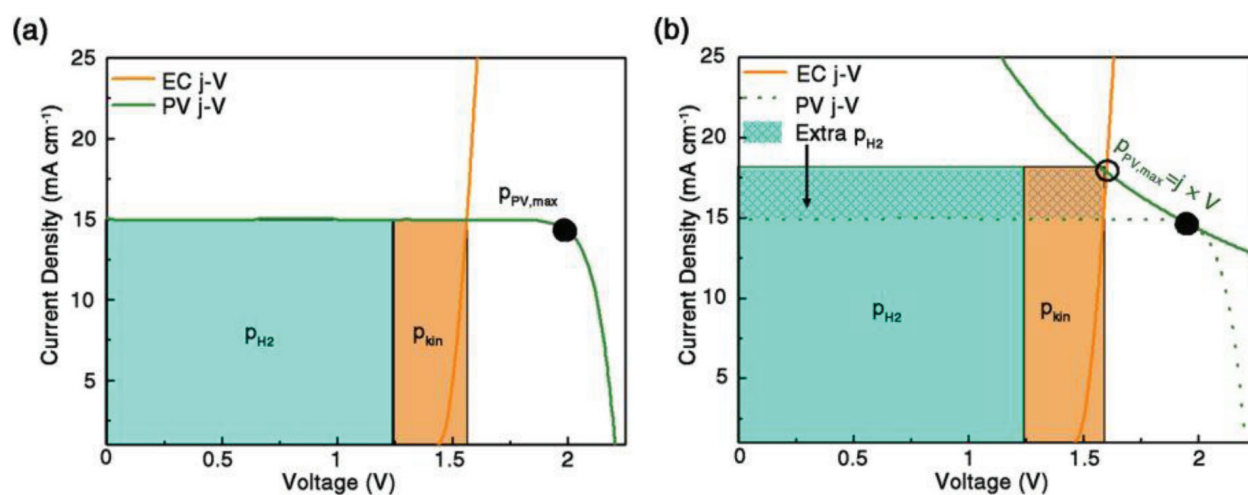

Figure 6. Design principle of the PV-Conv-EC system based on an independent PV, the EC performance, and the existence of a converter. (a) Hydrogen power per square centimeter (p_{H2}) and kinetic loss per square centimeter (p_{kin}) at a given current density–voltage (j − V) curve of the PV and EC. The intersection between the PV and EC j − V curve has a lower voltage and a higher current density than the $p_{PV, max point}$. (b) p_{H2} and p_{kin} after the DC-DC converter assistance on (a). Reproduced with permission [92]. Copyright (2015) American Chemical Society.

converter assistance, high STH efficiency PV-Conv-EC systems can achieve 20.6% STH efficiency and 78% PV electricity to hydrogen conversion efficiency [92].

Wind power is heavily influenced by meteorological variances and requires balancing power for the load fluctuation. Wind to hydrogen (WTH) strategies by water electrolysis could offer a solution to this problem [9]. Synergy between wind farms and water electrolyzers makes hydrogen a buffer solution to balance the grid power as well as produce hydrogen from surplus wind power [9]. Thus, the wind power can be utilized at its maximum capacity.

4.2. Current status of commercial manufacturers

Table 2 summarizes the commercially available PEM electrolysis systems from 12 major manufacturers worldwide. Note that only the highest capacity from each manufacturer is listed here. Six of the manufacturers are able to achieve a system capacity around 1 MW or higher. The largest system so far is from Hydrogenics, a 15 MW plant with 10 cell stacks capable of producing 3000 Nm^3 hydrogen per hour. Giner currently offers a more powerful cell stack, Kennebec stacks, even though its current systems have not yet incorporated this brand of the cell stack. The Kennebec stacks have the largest capacity among all the stacks available from these manufacturers. It has a capacity of 5 MW and is capable of producing 2200 kg of hydrogen per day (that is, 1020 Nm^3 per hour). Most of the systems offer high-purity hydrogen with the high delivery pressure that is suitable for on-site storage and fueling. The system consumption of electricity is very close among all the manufacturers, averaged around 5.5 ± 0.5 kWh per Nm^3 of hydrogen.

Manufacturers	System model	H2 production rate, Nm^3/hr	H2 purity (after purification)	Installed power, MW	System consumption, kWh/Nm^3 of H_2	Delivery pressure, bar	References
Hydrogenics	HyLYZER-3000	3000	99.998%	15	5.0–5.4	30	[93]
Proton Onsite	M400	400	>99.9995%	2	5	30	[94]
Siemens	Silyzer 200	225	99.9%	1.25	5.1–5.4	35	[95]
ITM power	HGas1000	215	99.999%	1.03	5.5	20–80	[96]
Giner	200S	200	99.999%	1	5	40	[97]
AREVA H2Gen	E120	120	99.999%	0.96	4.8	30	[98]
H-TEC	ME100/350	66	99.999%	0.225	4.9	20	[99]
Kobelco-eco solutions	SH60D	60	99.9999%	0.2	5.5–6.5	8.2	[100]
Treadwell Corp.	NA	10.2	NA	NA	NA	75.8	[101]
Angstrom Advanced	HGH170000	10	99.9999%	0.058	5.5	4	[102]
SylaTech	HE32	2	99.999%	0.01	4.9	30	[103]
GreenHydrogen	HyProvide P1	1	99.995%	0.01	5.5	50	[104]

Table 2. Summary of commercial PEM electrolysis systems.

5. Concluding remarks and outlook

The growing demand for energy and the accompanied environmental issues call for a rapid transition to low-carbon/carbon-free energy structure. In this context, hydrogen serves as an ideal secondary energy source for energy storage and transport. The key technology for hydrogen energy is water electrolysis. In particular, PEM electrolysis has been driven strongly by flexible energy storage in recent years as it offers several advantages compared to alkaline and solid oxide electrolysis. Nowadays, more mega-Watt scale PEM electrolysis systems are available on the market and in the field. However, further technological advancement is still demanded in the field of electrocatalysis and material science to obtain a deeper understanding of catalytic reactions and design new catalysts such that PEM electrolysis is more durable and cost-effective. Furthermore, as PEM electrolysis is but one building block for the future hydrogen economy, efforts in R&D should emphasize the compatibility with other technologies and optimize the synergic effects.

Conflict of interest

The authors have no conflict of interest to declare.

Author details

Radenka Maric[1,2] and Haoran Yu[1,2]*

*Address all correspondence to: haoran.yu@uconn.edu

1 Department of Chemical and Biomolecular Engineering, University of Connecticut, Storrs, CT, USA

2 Center for Clean Energy Engineering, University of Connecticut, Storrs, CT, USA

References

[1] Tverberg G. BP data suggests we are reaching peak energy demand. 2015. Available from: https://ourfiniteworld.com/2015/06/23/bp-data-suggests-we-are-reaching-peak-energy-demand [Accessed: April 14, 2018]

[2] Learning about renewable energy. Available from: https://www.nrel.gov/workingwithus/learning.html [Accessed: April 14, 2018]

[3] Vivas FJ, De las Heras A, Segura F, Andújar JM. A review of energy management strategies for renewable hybrid energy systems with hydrogen backup. Renewable and Sustainable Energy Reviews. 2018;**82**:126-155

[4]   Winsche WE, Hoffman KC, Salzano FJ. Hydrogen: Its Future Role in the Nation's Energy Economy. Science. 1973;**180**:1325

[5]   Bennaceur K, Clark B, Franklin MJ, Ramakrshnan TS, Roulet C, Stout E. Hydrogen: A future energy carrier? Oilfield Review. 2005;**17**:30-41

[6]   Mazloomi K, Gomes C. Hydrogen as an energy carrier: Prospects and challenges. Renewable and Sustainable Energy Reviews. 2012;**16**:3024-3033

[7]   Cipriani G, Di Dio V, Genduso F, La Cascia D, Liga R, Miceli R, et al. Perspective on hydrogen energy carrier and its automotive applications. International Journal of Hydrogen Energy. 2014;**39**:8482-8494

[8]   Sharma S, Ghoshal SK. Hydrogen the future transportation fuel: From production to applications. Renewable and Sustainable Energy Reviews. 2015;**43**:1151-1158

[9]   Hosseini SE, Wahid MA. Hydrogen production from renewable and sustainable energy resources: Promising green energy carrier for clean development. Renewable and Sustainable Energy Reviews. 2016;**57**:850-866

[10] Hanley ES, Deane J, Gallachóir BÓ. The role of hydrogen in low carbon energy futures—A review of existing perspectives. Renewable and Sustainable Energy Reviews. 2018;**82**: 3027-3045

[11] Buttler A, Spliethoff H. Current status of water electrolysis for energy storage, grid balancing and sector coupling via power-to-gas and power-to-liquids: A review. Renewable and Sustainable Energy Reviews. 2018;**82**:2440-2454

[12] Marshall A, Børresen B, Hagen H, Tsypkin M, Tunold R. Hydrogen production by advanced proton exchange membrane (PEM) water electrolysers—Reduced energy consumption by improved electrocatalysis. Energy. 2007;**32**:431-436

[13] Millet P, Ngameni R, Grigoriev SA, Mbemba N, Brisset F, Ranjbari A, et al. PEM water electrolyzers: From electrocatalysis to stack development. International Journal of Hydrogen Energy. 2010;**35**:5043-5052

[14] Millet P, Mbemba M, Grigoriev SA, Fateev VN, Aukauloo A, Etievant C. Electrochemical performances of PEM water electrolysis cells and perspectives. International Journal of Hydrogen Energy. 2011;**36**:4134-4142

[15] Carmo M, Fritz DL, Mergel J, Stolten D. A comprehensive review on PEM water electrolysis. International Journal of Hydrogen Energy. 2013;**38**:4901-4934

[16] Zafar S. Overview of Biomass Pyrolysis. 2018. Available from: https://www.bioenergyconsult.com/biomass-pyrolysis/ [Accessed: April 15, 2018]

[17] Møller KT, Jensen TR, Akiba E, Li H. Hydrogen - A sustainable energy carrier. Progress in Natural Science: Materials International. 2017;**27**:34-40

[18] Lototskyy MV, Tolj I, Pickering L, Sita C, Barbir F, Yartys V. The use of metal hydrides in fuel cell applications. Progress in Natural Science: Materials International. 2017;**27**:3-20

[19] Chen P, Zhu M. Recent progress in hydrogen storage. Materials Today. 2008;**11**:36-43

[20] Ursua A, Gandia LM, Sanchis P. Hydrogen production from water electrolysis: Current status and future trends. Proceedings of the IEEE. 2012;**100**:410-426

[21] Zhang Y, Lundblad A, Campana PE, Yan J. Comparative study of battery storage and hydrogen storage to increase photovoltaic self-sufficiency in a residential building of Sweden. Energy Procedia. 2016;**103**:268-273

[22] Fabbri E, Habereder A, Waltar K, Kotz R, Schmidt TJ. Developments and perspectives of oxide-based catalysts for the oxygen evolution reaction. Catalysis Science & Technology. 2014;**4**:3800-3821

[23] Reier T, Nong HN, Teschner D, Schlogl R, Strasser P. Electrocatalytic oxygen evolution reaction in acidic environments: Reaction mechanisms and catalysts. Advanced Energy Materials. 2017;**7**. 1601275

[24] Ayers KE, Anderson EB, Capuano C, Carter B, Dalton L, Hanlon G, et al. Research advances towards low cost, high efficiency PEM electrolysis. ECS Transactions. 2010;**33**:3-15

[25] Danilovic N, Ayers KE, Capuano C, Renner JN, Wiles L, Pertoso M. (Plenary) Challenges in going from laboratory to megawatt scale PEM electrolysis. ECS Transactions. 2016;**75**:395-402

[26] Spori C, Kwan JTH, Bonakdarpour A, Wilkinson DP, Strasser P. The stability challenges of oxygen evolving catalysts: Towards a common fundamental understanding and mitigation of catalyst degradation. Angewandte Chemie International Edition. 2017;**56**:5994-6021

[27] Danilovic N, Subbaraman R, Chang KC, Chang SH, Kang Y, Snyder J, et al. Using surface segregation to design stable Ru-Ir oxides for the oxygen evolution reaction in acidic environments. Angewandte Chemie International Edition. 2014;**53**:14016-14021

[28] Danilovic N, Subbaraman R, Chang K, Chang SH, Kang YJ, Snyder J, et al. Activity-stability trends for the oxygen evolution reaction on monometallic oxides in acidic environments. Journal of Physical Chemistry Letters. 2014;**5**:2474-2478

[29] Fierro S, Kapałka A, Comninellis C. Electrochemical comparison between IrO_2 prepared by thermal treatment of iridium metal and IrO_2 prepared by thermal decomposition of H_2IrCl_6 solution. Electrochemistry Communications. 2010;**12**:172-174

[30] Reier T, Teschner D, Lunkenbein T, Bergmann A, Selve S, Kraehnert R, et al. Electrocatalytic oxygen evolution on iridium oxide: Uncovering catalyst-substrate interactions and active iridium oxide species. Journal of the Electrochemical Society. 2014;**161**:F876-F882

[31] Geiger S, Kasian O, Shrestha BR, Mingers AM, Mayrhofer KJJ, Cherevko S. Activity and stability of electrochemically and thermally treated iridium for the oxygen evolution reaction. Journal of the Electrochemical Society. 2016;**163**:F3132-F3138

[32] Cherevko S, Reier T, Zeradjanin AR, Pawolek Z, Strasser P, Mayrhofer KJJ. Stability of nanostructured iridium oxide electrocatalysts during oxygen evolution reaction in acidic environment. Electrochemistry Communications. 2014;**48**:81-85

[33] Xu J, Wang M, Liu G, Li J, Wang X. The physical–chemical properties and electrocatalytic performance of iridium oxide in oxygen evolution. Electrochimica Acta. 2011;**56**:10223-10230

[34] Abbott DF, Lebedev D, Waltar K, Povia M, Nachtegaal M, Fabbri E, et al. Iridium oxide for the oxygen evolution reaction: Correlation between particle size, morphology, and the surface hydroxo layer from operando XAS. Chemistry of Materials. 2016;**28**:6591-6604

[35] Chandra D, Takama D, Masaki T, Sato T, Abe N, Togashi T, et al. Highly efficient electrocatalysis and mechanistic investigation of intermediate IrOx(OH)y nanoparticle films for water oxidation. ACS Catalysis. 2016;**6**:3946-3954

[36] Pfeifer V, Jones TE, Velasco Velez JJ, Massue C, Arrigo R, Teschner D, et al. The electronic structure of iridium and its oxides. Surface and Interface Analysis. 2016;**48**:261-273

[37] Minguzzi A, Lugaresi O, Achilli E, Locatelli C, Vertova A, Ghigna P, et al. Observing the oxidation state turnover in heterogeneous iridium-based water oxidation catalysts. Chemical Science. 2014;**5**:3591-3597

[38] Minguzzi A, Locatelli C, Lugaresi O, Achilli E, Cappelletti G, Scavini M, et al. Easy Accommodation of different oxidation states in iridium oxide nanoparticles with different hydration degree as water oxidation electrocatalysts. ACS Catalysis. 2015;**5**:5104-5115

[39] Cherevko S, Geiger S, Kasian O, Mingers A, Mayrhofer KJJ. Oxygen evolution activity and stability of iridium in acidic media. Part 2. – Electrochemically grown hydrous iridium oxide. Journal of Electroanalytical Chemistry. 2016;**774**:102-110

[40] Grigoriev SA, Bessarabov DG, Fateev VN. Degradation mechanisms of MEA characteristics during water electrolysis in solid polymer electrolyte cells. Russian Journal of Electrochemistry. 2017;**53**:318-323

[41] Rozain C, Mayousse E, Guillet N, Millet P. Influence of iridium oxide loadings on the performance of PEM water electrolysis cells: Part II. – Advanced oxygen electrodes, Applied Catalysis B: Environmental. 2016;**182**:123-131

[42] Siracusano S, Baglio V, Grigoriev SA, Merlo L, Fateev VN, Aricò AS. The influence of iridium chemical oxidation state on the performance and durability of oxygen evolution catalysts in PEM electrolysis. Journal of Power Sources. 2017;**366**:105-114

[43] Rakousky C, Reimer U, Wippermann K, Carmo M, Lueke W, Stolten D. An analysis of degradation phenomena in polymer electrolyte membrane water electrolysis. Journal of Power Sources. 2016;**326**:120-128

[44] Lettenmeier P, Wang R, Abouatallah R, Helmly S, Morawietz T, Hiesgen R, et al. Durable membrane electrode assemblies for proton exchange membrane electrolyzer systems operating at high current densities. Electrochimica Acta. 2016;**210**:502-511

[45] Lewinski KA, van dV, Luopa SM. NSTF advances for PEM electrolysis - the effect of alloying on activity of NSTF electrolyzer catalysts and performance of NSTF based PEM electrolyzers. ECS Transactions. 2015;**69**:893-917

[46] Wang L, Saveleva VA, Zafeiratos S, Savinova ER, Lettenmeier P, Gazdzicki P, et al. Highly active anode electrocatalysts derived from electrochemical leaching of Ru from metallic $Ir_{0.7}Ru_{0.3}$ for proton exchange membrane electrolyzers. Nano Energy. 2017;**34**: 385-391

[47] Siracusano S, Hodnik N, Jovanovic P, Ruiz-Zepeda F, Šala M, Baglio V, et al. New insights into the stability of a high performance nanostructured catalyst for sustainable water electrolysis. Nano Energy. 2017;**40**:618-632

[48] Liu G, Xu J, Wang Y, Wang X. An oxygen evolution catalyst on an antimony doped tin oxide nanowire structured support for proton exchange membrane liquid water electrolysis. Journal of Materials Chemistry A. 2015;**3**:20791-20800

[49] Damjanovic A, Dey A, Bockris JO. Kinetics of oxygen evolution and dissolution on platinum electrodes. Electrochimica Acta. 1966;**11**:791-814

[50] Damjanovic A, Wong MKY. On the mechanism of oxygen evolution at iridium electrodes. Journal of The Electrochemical Society. 1967;**114**:592-593

[51] Busch M, Ahlberg E, Panas I. Electrocatalytic oxygen evolution from water on a Mn(iii-v) dimer model catalyst-A DFT perspective. Physical Chemistry Chemical Physics. 2011;**13**: 15069-15076

[52] Steegstra P, Busch M, Panas I, Ahlberg E. Revisiting the redox properties of hydrous iridium oxide films in the context of oxygen evolution. Journal of Physical Chemistry C. 2013;**117**:20975-20981

[53] Cherevko S, Geiger S, Kasian O, Mingers A, Mayrhofer KJJ. Oxygen evolution activity and stability of iridium in acidic media. Part 1. – Metallic iridium. Journal of Electroanalytical Chemistry. 2016;**773**:69-78

[54] Xu D, Diao P, Jin T, Wu Q, Liu X, Guo X, et al. Iridium oxide nanoparticles and iridium/iridium oxide nanocomposites: Photochemical fabrication and application in catalytic reduction of 4-nitrophenol. ACS Applied Materials & Interfaces. 2015;**7**:16738-16749

[55] Cruz AM, Abad L, Carretero NM, Moral-Vico J, Fraxedas J, Lozano P, et al. Iridium oxohydroxide, a significant member in the family of iridium oxides. Stoichiometry, characterization, and implications in bioelectrodes. Journal of Physical Chemistry C. 2012;**116**:5155-5168

[56] Sanchez Casalongue HG, Ng ML, Sarp K, Daniel F, Hirohito O, Anders N. In Situ observation of surface species on iridium oxide nanoparticles during the oxygen evolution reaction. Angewandte Chemie International Edition. 2014;**53**:7169-7172

[57] Pfeifer V, Jones TE, Velasco Velez JJ, Arrigo R, Piccinin S, Havecker M, et al. In situ observation of reactive oxygen species forming on oxygen-evolving iridium surfaces. Chemical Science. 2017;**8**:2143-2149

[58] Massue C, Pfeifer V, van Gastel M, Noack J, Algara-Siller G, Cap S, et al. Reactive electrophilic O^{I-} species evidenced in high-performance iridium oxohydroxide water oxidation electrocatalysts. ChemSusChem. 2017;**10**:4786-4798

[59] Pfeifer V, Jones TE, Wrabetz S, Massue C, Velasco Velez JJ, Arrigo R, et al. Reactive oxygen species in iridium-based OER catalysts. Chemical Science. 2016;**7**:6791-6795

[60] Cyriac M, Verena P, Xing H, Johannes N, Andrey T, Sébastien C, et al. High-performance supported iridium oxohydroxide water oxidation electrocatalysts. ChemSusChem. 2017;**10**:1943-1957

[61] Pfeifer V, Jones TE, Velasco Velez JJ, Massue C, Greiner MT, Arrigo R, et al. The electronic structure of iridium oxide electrodes active in water splitting. Physical Chemistry Chemical Physics. 2016;**18**:2292-2296

[62] Bernicke M, Ortel E, Reier T, Bergmann A, Ferreira de Araujo J, Strasser P, et al. Iridium oxide coatings with templated porosity as highly active oxygen evolution catalysts: Structure-activity relationships. ChemSusChem. 2015;**8**:1908-1915

[63] Oh HS, Nong HN, Reier T, Bergmann A, Gliech M, Ferreira de Araújo J, et al. Electrochemical catalyst – support effects and their stabilizing role for IrOx nanoparticle catalysts during the oxygen evolution reaction. Journal of the American Chemical Society. 2016;**138**:12552-12563

[64] Oakton E, Lebedev D, Povia M, Abbott DF, Fabbri E, Fedorov A, et al. IrO_2-TiO_2: A high-surface-area, active, and stable electrocatalyst for the oxygen evolution reaction. ACS Catalysis. 2017;**7**:2346-2352

[65] De Pauli CP, Trasatti S. Composite materials for electrocatalysis of O_2 evolution: IrO_2+SnO_2 in acid solution. Journal of Electroanalytical Chemistry. 2002;**538–539**:145-151

[66] Petrykin V, Macounová K, Okube M, Mukerjee S, Krtil P. Local structure of Co doped RuO_2 nanocrystalline electrocatalytic materials for chlorine and oxygen evolution. Catalysis Today. 2013;**202**:63-69

[67] Kadakia K, Datta MK, Velikokhatnyi OI, Jampani PH, Kumta PN. Fluorine doped (Ir,Sn,Nb)O_2 anode electro-catalyst for oxygen evolution via PEM based water electrolysis. International Journal of Hydrogen Energy. 2014;**39**:664-674

[68] González-Huerta RG, Ramos-Sánchez G, Balbuena PB. Oxygen evolution in Co-doped RuO_2 and IrO_2: Experimental and theoretical insights to diminish electrolysis overpotential. Journal of Power Sources. 2014;**268**:69-76

[69] Reier T, Pawolek Z, Cherevko S, Bruns M, Jones T, Teschner D, et al. Molecular insight in structure and activity of highly efficient, low-Ir Ir-Ni oxide catalysts for electrochemical water splitting (OER). Journal of the American Chemical Society. 2015;**137**:13031-13040

[70] Tae EL, Song J, Lee AR, Kim CH, Yoon S, Hwang IC, et al. Cobalt oxide electrode doped with iridium oxide as highly efficient water oxidation electrode. ACS Catalysis. 2015;**5**: 5525-5529

[71] Tran V, Yatabe T, Matsumoto T, Nakai H, Suzuki K, Enomoto T, et al. An IrSi oxide film as a highly active water-oxidation catalyst in acidic media. Chemical Communications. 2015;**51**: 12589-12592

[72] Yu A, Lee C, Kim MH, Lee Y. Nanotubular iridium-cobalt mixed oxide crystalline architectures inherited from cobalt oxide for highly efficient oxygen evolution reaction catalysis. ACS Applied Materials & Interfaces. 2017;**9**:35057-35066

[73] Sun W, Song Y, Gong X, Cao L, Yang J. An efficiently tuned d-orbital occupation of IrO_2 by doping with Cu for enhancing the oxygen evolution reaction activity. Chemical Science. 2015;**6**:4993-4999

[74] Mason MG, Gerenser LJ, Lee S-T. Electronic structure of catalytic metal clusters studied by x-ray photoemission spectroscopy. Physical Review Letters. 1977;**39**:288-291

[75] Mason MG. Electronic structure of supported small metal clusters. Physical Review B. 1983;**27**:748-762

[76] Wertheim GK, DiCenzo SB, Buchanan DNE. Noble- and transition-metal clusters: The d bands of silver and palladium. Physical Review B. 1986;**33**:5384-5390

[77] Sun CQ. Surface and nanosolid core-level shift: Impact of atomic coordination-number imperfection. Physical Review B. 2004;**69**:045105

[78] Richter B, Kuhlenbeck H, Freund H-J, Bagus PS. Cluster core-level binding-energy shifts: The role of lattice strain. Physical Review Letters. 2004;**93**:026805

[79] Zhou WP, Lewera A, Larsen R, Masel RI, Bagus PS, Wieckowski A. Size effects in electronic and catalytic properties of unsupported palladium nanoparticles in electrooxidation of formic acid. The Journal of Physical Chemistry. B. 2006;**110**:13393-13398

[80] Litster S, McLean G. PEM fuel cell electrodes. Journal of Power Sources. 2004;**130**:61-76

[81] Holdcroft S. Fuel cell catalyst layers: A polymer science perspective. Chemistry of Materials. 2014;**26**:381-393

[82] Ma L, Sui S, Zhai Y. Investigations on high performance proton exchange membrane water electrolyzer. International Journal of Hydrogen Energy. 2009;**34**:678-684

[83] Xu W, Scott K. The effects of ionomer content on PEM water electrolyser membrane electrode assembly performance. International Journal of Hydrogen Energy. 2010;**35**: 12029-12037

[84] Ma H, Liu C, Liao J, Su Y, Xue X, Xing W. Study of ruthenium oxide catalyst for electrocatalytic performance in oxygen evolution. Journal of Molecular Catalysis A: Chemical. 2006;**247**:7-13

[85] Bernt M, Gasteiger HA. Influence of ionomer content in IrO_2/TiO_2 electrodes on PEM water electrolyzer performance. Journal of the Electrochemical Society. 2016;**163**:F3179-F3189

[86] Park S, Shao Y, Liu J, Wang Y. Oxygen electrocatalysts for water electrolyzers and reversible fuel cells: status and perspective. Energy & Environmental Science. 2012;**5**: 9331-9344

[87] Holladay JD, Hu J, King DL, Wang Y. An overview of hydrogen production technologies. Catalysis Today. 2009;**139**:244-260

[88] Arico AS, Siracusano S, Briguglio N, Baglio V, Di Blasi A, Antonucci V. Polymer electrolyte membrane water electrolysis: status of technologies and potential applications in combination with renewable power sources. Journal of Applied Electrochemistry. 2013; **43**:107-118

[89] Götz M, Lefebvre J, Mörs F, McDaniel Koch A, Graf F, Bajohr S, et al. Renewable power-to-gas: A technological and economic review. Renewable Energy. 2016;**85**:1371-1390

[90] Schiebahn S, Grube T, Robinius M, Tietze V, Kumar B, Stolten D. Power to gas: Technological overview, systems analysis and economic assessment for a case study in Germany. International Journal of Hydrogen Energy. 2015;**40**:4285-4294

[91] Chang WJ, Lee KH, Ha JI, Nam KT. Hydrogen production via water electrolysis: The benefits of a solar cell-powered process. IEEE Electrification Magazine. 2018;**6**:19-25

[92] Chang WJ, Lee K, Ha H, Jin K, Kim G, Hwang S, et al. Design principle and loss engineering for photovoltaic-electrolysis cell system. ACS Omega. 2017;**2**:1009-1018

[93] Hydrogenics. Hydrogenics Renewable Hydrogen Solutions. Available from: http://www.hydrogenics.com/wp-content/uploads/Renewable-Hydrogen-Brochure.pdf [Accessed: April 12, 2018]

[94] Proton Onsite. High Capacity Hydrogen Systems: M Series PEM Electrolyzers. Available from: http://www.protononsite.com/sites/default/files/2016-10/pd-0600-0114_rev_a.pdf [Accessed: April 14, 2018]

[95] Siemens. Available from: https://www.industry.siemens.com/topics/global/en/pem-electrolyzer/silyzer/silyzer-systems/Pages/silyzer-systeme1105-9496.aspx [Accessed: April 14, 2018]

[96] ITM-power. Available from: http://www.itm-power.com/product/hgas [Accessed: April 14, 2018]

[97] Giner. Available from: https://www.ginerelx.com/electrolyzer-systems [Accessed: April 14, 2018]

[98] Arevah2gen. Available from: http://www.arevah2gen.com/wpcontent/uploads/2017/02/AREVA_H2GEN_FICHE_PRODUIT_FRANCE_HD.pdf [Accessed: April 14, 2018]

[99] H-TEC. Available from: https://www.h-tec-systems.com/fileadmin/Content/PDFs/24022018/HTEC_SYSTEMS_Datasheet_Series-ME_24022018.pdf [Accessed: April 14, 2018]

[100] Kobelco-eco. Available from: http://www.kobelco-eco.co.jp/product/suisohassei/img/catalog_hhog.pdf. [Accessed: April 14, 2018]

[101] Treadwell Corp. Available from: http://www.treadwellcorp.com/proton-exchange-membrane-hydrogen-generator.php [Accessed: April 14, 2018]

[102] Angstrom-advanced. Available from: http://www.angstrom-advanced.com/index.asp?page=HGH10000 [Accessed: April 14, 2018]

[103] Sylatech. Available from: http://www.sylatech.de/pdf/Elektrolyseure.pdf [Accessed: April 14, 2018]

[104] Greenhydrogen. Available from: http://greenhydrogen.dk/technology/hyprovide/ [Accessed: April 14, 2018]